

Imbalances in protein homeostasis caused by mutant desmin

L. Winter^{*†}, A. Unger^{‡§}, C. Berwanger^{¶**}, M. Spörrer^{††}, M. Türk^{‡‡}, F. Chevessier^{*}, K.-H. Strucksberg^{**}, U. Schlötzer-Schrehardt^{§§}, I. Wittig^{¶¶}, W. H. Goldmann^{††}, K. Marcus^{***}, W. A. Linke^{†††}, C. S. Clemen^{¶**·1}  and R. Schröder^{*·1}

^{*}Institute of Neuropathology, University Hospital Erlangen, Erlangen, Germany, [†]Neuromuscular Research Department, Center for Anatomy and Cell Biology, Medical University of Vienna, Vienna, Austria, [‡]Department of Cardiovascular Physiology, Ruhr-University Bochum, Bochum, Germany, [§]Institute for Genetics of Heart Diseases, University Hospital Münster, Münster, Germany, [¶]Department of Neurology, Heimer Institute for Muscle Research, University Hospital Bergmannsheil, Ruhr-University Bochum, Bochum, Germany, ^{**}Center for Biochemistry, Institute of Biochemistry I, Medical Faculty, University of Cologne, Cologne, Germany, ^{††}Center for Medical Physics and Technology, Biophysics Group, Friedrich-Alexander-University Erlangen-Nuremberg, Erlangen, Germany, ^{‡‡}Department of Neurology, ^{§§}Department of Ophthalmology, University Hospital Erlangen, Erlangen, Germany, ^{¶¶}Functional Proteomics, SFB815 Core Unit, Medical School, Goethe University, Frankfurt, Germany, ^{***}Medizinisches Proteom-Center, Medical Faculty, Ruhr-University Bochum, Bochum and ^{†††}Institute of Physiology II, University of Münster, Münster, Germany

L. Winter, A. Unger, C. Berwanger, M. Spörrer, M. Türk, F. Chevessier, K.-H. Strucksberg, U. Schlötzer-Schrehardt, I. Wittig, W. H. Goldmann, K. Marcus, W. A. Linke, C. S. Clemen and R. Schröder (2018) *Neuropathology and Applied Neurobiology*

Imbalances in protein homeostasis caused by mutant desmin

Aims: We investigated newly generated immortalized heterozygous and homozygous R349P desmin knock-in myoblasts in conjunction with the corresponding desminopathy mice as models for desminopathies to analyse major protein quality control processes in response to the presence of R349P mutant desmin. **Methods:** We used hetero- and homozygous R349P desmin knock-in mice for analyses and for crossbreeding with p53 knock-out mice to generate immortalized R349P desmin knock-in skeletal muscle myoblasts and myotubes. Skeletal muscle sections and cultured muscle cells were investigated by indirect

immunofluorescence microscopy, proteasomal activity measurements and immunoblotting addressing autophagy rate, chaperone-assisted selective autophagy and heat shock protein levels. Muscle sections were further analysed by transmission and immunogold electron microscopy. **Results:** We demonstrate that mutant desmin (i) increases proteasomal activity, (ii) stimulates macroautophagy, (iii) dysregulates the chaperone assisted selective autophagy and (iv) elevates the protein levels of α B-crystallin and Hsp27. Both α B-crystallin and Hsp27 as well as Hsp90 displayed translocation patterns from Z-discs as well as Z-I junctions, respectively, to the level of sarcomeric I-bands in dominant and recessive desminopathies. **Conclusions:** Our findings demonstrate that the presence of R349P mutant desmin causes a general imbalance in skeletal muscle protein homeostasis via aberrant activity of all major protein quality control systems. The augmented activity of these systems and the subcellular shift of essential heat shock proteins may deleteriously contribute to the previously observed increased turnover of desmin itself and desmin-binding

Correspondence: Christoph S. Clemen, Department of Neurology, Heimer Institute for Muscle Research, University Hospital Bergmannsheil, Ruhr-University Bochum, Bürkle-de-la-Camp-Platz 1, 44789 Bochum, Germany or Rolf Schröder, Institute of Neuropathology, University Hospital Erlangen, Schwabachanlage 6, 91054 Erlangen, Germany. Tel: +49 234 302 7541 or +49 9131 85 34782; Fax: +49 234 302 6888 or +49 9131 85 26033; E-mail: christoph.clemen@rub.de or rolf.schroeder@uk-erlangen.de

¹Both authors contributed equally to this work.

© 2018 The Authors. *Neuropathology and Applied Neurobiology* published by John Wiley & Sons Ltd on behalf of British Neuropathological Society.

This is an open access article under the terms of the Creative Commons Attribution-NonCommercial-NoDerivs License, which permits use and distribution in any medium, provided the original work is properly cited, the use is non-commercial and no modifications or adaptations are made.

partners, which triggers progressive dysfunction of the extrasarcomeric cytoskeleton and the myofibrillar apparatus in the course of the development of desminopathies.

Keywords: desminopathy, immortalized myoblasts, protein homeostasis, protein quality control, R349P desmin knock-in mice

apparatus in the course of the development of desminopathies.

Introduction

The term 'desminopathies' refers to a clinically heterogeneous group of familial and sporadic myopathies and cardiomyopathies that are caused by mutations of the human desmin (*DES*) gene on chromosome 2q35. Desmin, the muscle-specific intermediate filament protein, is a major component of the three-dimensional extrasarcomeric cytoskeleton, which exerts multiple roles in the alignment and anchorage of myofibrils, the positioning of mitochondria and myonuclei, mechanosensation, stress endurance and cell signalling [1–4]. The vast majority of desminopathies follows an autosomal-dominant trait of inheritance; the few autosomal-recessive cases may be subdivided in cases with maintained expression of mutant desmin [5–9] and others with a complete lack of desmin [10–13]. The morphological hallmark of desminopathies with maintained desmin protein expression is the presence of sarcoplasmic and subsarcolemmal desmin-positive protein aggregates in conjunction with degenerative changes of the myofibrillar apparatus [1].

Molecular studies on human desminopathies are generally hampered by the very limited amount of available human muscle tissue specimens and the fact that the alterations noticed in diagnostic muscle biopsies nearly always reflect late stages of the disease. Moreover, diagnostic human muscle biopsies are highly heterogeneous with regard to age, sex, biopsied muscles and disease severity of individual patients. To overcome these limitations, the availability of cell and animal models closely mirroring the human disease pathology is important. As a patient-mimicking desminopathy model, we reported a R349P desmin knock-in mouse model, which harbours the ortholog of the most frequent human desmin mutation R350P. This desminopathy model develops age-dependent desmin-positive protein aggregation pathology, skeletal muscle weakness, dilated cardiomyopathy as well as cardiac arrhythmias and conduction defects [14]. However, for studies on the level of single myoblasts

and myotubes, there is still a major need for an appropriate and reproducible desminopathy cell model. Though human primary myoblast cultures derived from diagnostic skeletal muscle biopsies of desminopathy patients are available, they have the following disadvantages, (i) they consist of heterogeneous mixtures of myoblasts and fibroblasts, (ii) the contaminating fibroblasts become the predominant cell type after a few passages and (iii) the myogenic cells display a limited mitotic capacity and lifespan. Consequently, repeated muscle biopsy sampling from patients with subsequent isolation of muscle cells would be needed. Beyond ethical problems, this approach would also increase the inter-experimental variability and thus is far from being optimal and practical. As an alternative approach, we generated immortalized heterozygous and homozygous R349P desminopathy as well as wild-type myoblast cultures, which were established by crossbreeding our R349P desmin knock-in mouse line [14] with p53 knock-out mice [15] followed by subsequent isolation of myoblast cells from skeletal muscles.

Previous studies demonstrated changes in various aspects of protein homeostasis in desminopathies and other forms of protein aggregate myopathies (for review see [14]). While these studies mostly addressed single aspects of protein quality control systems, the here presented study provides a comprehensive analysis of the ubiquitin-proteasome system, bulk autophagy, chaperone-assisted selective autophagy (CASA) and heat shock protein levels and their intracellular localization in our newly generated heterozygous and homozygous immortalized desminopathy myoblasts in conjunction with skeletal muscle tissue from the respective desminopathy mice.

Materials and Methods

Animals

In the present study, we used 3-month-old (unless stated otherwise) hetero- and homozygous R349P

(c.1045_1047delAGG>insCCC) desmin knock-in mice B6J.129Sv-Des^{tm1.1Ccrs} (<http://www.informatics.jax.org/allele/MGI:5708562>) [14] and their wild-type siblings as well as p53 knock-out mice B6.129S2-Trp53^{tm1Tyj} (<http://www.informatics.jax.org/allele/MGI:1857263>) [15]. Mice were handled in accordance with the German Animal Welfare Act (Tierschutzgesetz) as well as the German Regulation for the protection of animals used for experimental purposes or other scientific purposes (Tierschutz-Versuchstierverordnung). All investigations were approved by the governmental office for animal care [Landesamt für Natur, Umwelt und Verbraucherschutz North Rhine-Westphalia, Recklinghausen, Germany (reference numbers 84-02.04.2014, A262 and 84-02.05.40.14.057); Regierung von Mittelfranken, Ansbach, Germany (reference number TF-14/2015)].

Generation and cultivation of immortalized myoblasts

For the generation of immortalized myoblast cell lines according to [16], homozygous R349P desmin knock-in mice [14] were cross-bred with homozygous p53 knock-out mice [15] to generate offspring double-heterozygous for the R349P desmin knock-in and p53 knock-out alleles. These mice were further mated to obtain offspring with the following genotypes for the isolation of skeletal muscle myoblasts, homozygous R349P desmin knock-in and homozygous p53 knock-out, heterozygous R349P desmin knock-in and homozygous p53 knock-out, wild-type desmin and homozygous p53 knock-out alleles.

Myoblast isolation was performed according to a protocol modified from [17,18]. De-skinned soleus muscles from 8-week-old mice were enzymatically dissociated in 6 ml enzyme solution (0.2% of collagenase I in DMEM) for 1.5–2 h at 37°C and gentle agitation. The digested tissue was poured into a 55 mm cell culture dish containing 6 ml pre-warmed DMEM, and single muscle fibres were released by gentle trituration with a Pasteur pipette. Cell culture dishes and glass pipettes were pre-flushed with 10% of horse serum in DMEM. Once 20–30 intact fibres were separated, the muscle bulk was transferred to a fresh dish. The previous dish, containing separated fibres and debris, was stored in the incubator at 37°C and 5% of CO₂. The fibre separation cycle was

repeated until sufficient numbers of fibres had been dissociated from the muscle. The intact muscle fibres were then separated from the debris by transferring them in a Pasteur pipette to a dish, which had been coated with Matrigel (diluted 1:100 in DMEM; BD Biosciences, Franklin Lakes, New Jersey, USA). The plated fibres were allowed to settle and attach for 3 min to the Matrigel substrate, and then 1 ml plating medium (DMEM containing 10% of horse serum and 0.5% of chicken embryo extract) was slowly added to each dish. Plates were returned to the incubator at 37°C and 5% of CO₂ for 24 h to allow the growth of skeletal muscle myoblasts dissociating from the isolated muscle fibres. Myoblasts were split, pre-plated on uncoated culture dishes for up to 2 h in order to remove contaminating fibroblasts (a procedure performed at every splitting), and finally cultivated in Ham's F10 medium supplemented with 20% of foetal calf serum, 2.5 ng/ml basic fibroblast growth factor (Promega, Madison, Wisconsin, USA), 50 U/ml penicillin and 50 µg/ml streptomycin on collagen-coated (0.01% of collagen in PBS) culture dishes. To induce differentiation, growth medium was exchanged by differentiation medium (DMEM containing 5% of horse serum, 50 U/ml penicillin and 50 µg/ml streptomycin). The R349P desmin knock-in and p53 knock-out genotypes of each myoblast culture were verified by PCR. Immortalized myoblast cell lines with passage numbers of up to 40 were used for the experiments.

Antibodies

The following primary antibodies were used for immunodetection:

- desmin (both wild-type and mutant desmin, 'total' desmin), mouse monoclonal, 1:1000 in PBS-T for immunoblotting, 1:100 in PBS for immunofluorescence microscopy, clone D33, Dako/Agilent, Santa Clara, California, USA
- desmin ('total' desmin), rabbit monoclonal, 1:100 in PBS for immunofluorescence microscopy, #5332, Cell Signalling, Danvers, Massachusetts, USA
- R349P point-mutant desmin, rabbit polyclonal, 1:1000 in PBS-T for immunoblotting, [14]
- GAPDH, rabbit polyclonal, 1:10 000 in PBS-T for immunoblotting, G9545, Sigma-Aldrich, St. Louis, Missouri, USA

- α -actinin 2 (sarcomeric α -actinin), mouse monoclonal, 1:700 in PBS for immunofluorescence microscopy, A7732, Sigma-Aldrich
- ubiquitin, rabbit polyclonal, 1:1000 in PBS-T for immunoblotting, ab7780, Abcam, Cambridge, UK
- 19S proteasome subunit 4 (Rpt2), rabbit polyclonal, 1:1000 in PBS-T for immunoblotting, #09-280, Upstate/Fisher Scientific, Hampton, New Hampshire, USA
- actin, mouse monoclonal, 1:1000 in PBS-T for immunoblotting, A4700, Sigma-Aldrich
- light chain 3B (LC3B), rabbit monoclonal, 1:100 in PBS for immunofluorescence microscopy, 1:1000 in PBS-T for immunoblotting, #3868, Cell Signalling
- ULK1, rabbit polyclonal, 1:500 in PBS-T for immunoblotting
- sequestosome 1 (SQSTM1)/p62, rabbit polyclonal, 1:3000 in PBS-T for immunoblotting, P0067, Sigma-Aldrich
- filamin-C, rabbit polyclonal, 1:10 000 in PBS-T for immunoblotting, d16-20, kindly provided by D. Fürst, Bonn, Germany [19]
- BAG-3, rabbit polyclonal, 1:3000 in PBS-T for immunoblotting, 10599-1-AP, Proteintech, Manchester, UK
- α B-crystallin, rabbit polyclonal antibody, 1:1,000 in PBS-T for immunoblotting, SPA-223, Stressgen/Enzo Life Sciences, Lörrach, Germany
- α B-crystallin, rabbit polyclonal antibody, 1:250 for immunoelectron microscopy, SMC 1653A10, StressMarq Biosciences, Victoria, British Columbia, Canada
- α B-crystallin, rabbit polyclonal antibody, 1:400 for immunoelectron microscopy, SR 223F, MBL, Woburn, Massachusetts, USA
- Hsp27, rabbit polyclonal antibody, 1:1000 in PBS-T for immunoblotting, ab12351, Abcam
- Hsp27, rabbit polyclonal antibody, 1:250 for immunoelectron microscopy, SMC 1615D12, StressMarq Biosciences
- Hsp27, rabbit polyclonal antibody, 1:200 for immunoelectron microscopy, SR B800, MBL
- Hsp90 (total), rabbit monoclonal, 1:1000 in PBS-T for immunoblotting, 1:400 for immunoelectron microscopy, #4877, Cell Signalling
- Hsp90-alpha, rabbit polyclonal, 1:500 for immunoelectron microscopy, Pineda [20]
- titin (PEVK domain), mouse monoclonal, 1:200 for immunoelectron microscopy, #9D10, Developmental

Studies Hybridoma Bank, University of Iowa, Iowa City, Iowa, USA.

Secondary antibodies were HRP-conjugated (Biorad, Hercules, California, USA) for immunoblot analyses, donkey anti-mouse IgG Alexa Fluor 555, goat anti-mouse IgG Alexa Fluor 488, donkey anti-rabbit IgG Alexa Fluor 488 and goat anti-rabbit IgG Alexa Fluor 555 (Life Technologies, Carlsbad, California, USA) as well as anti-rabbit IgG Cy3 and anti-mouse IgG FITC (Rockland Immunochemicals, Limerick, Pennsylvania, USA) for immunofluorescence imaging, and anti-rabbit/mouse IgG F(ab')₂ Gold 1.4 nm (Nanoprobes, Stony Brook, New York, USA) for immunoelectron microscopy.

Preparation of tissue and cell lysates for SDS-PAGE

Dissected muscles (gastrocnemius and soleus) were snap frozen in liquid nitrogen, ground in a mortar, and taken up in lysis buffer [5 mM Tris-HCl pH 6.8, 10% of SDS, 0.2 M DTT, 1 mM EDTA, 100 mM NaF, 50 mM β -glycerophosphate, 2 mM Na₃VO₄, 1 mM PMSF, Complete mini protease inhibitor cocktail (Roche, Basel, Switzerland)] according to [17]; per 10 mg of muscle, 100 μ l of the buffer were used. Homogenization was performed using a Dounce tissue grinder. The homogenate was centrifuged for 10 min at 10 000 *g*, the supernatant was mixed with 6 \times SDS sample buffer (500 mM Tris-HCl pH 6.8, 600 mM DTT, 10% SDS, 0.1% of Bromophenol-blue, 30% of glycerol), incubated at 95°C for 5 min and stored at -20°C (protocol modified from [21]).

Cells were directly scraped off in 6 \times SDS sample buffer, DNA sheared by pressing the lysates through a 27-gauge needle, and samples were incubated for 5 min at 95°C and stored at -20°C. For proteasome inhibition prior to cell lysis, the differentiation medium was supplemented with 10 μ M MG132 (Sigma-Aldrich) overnight.

Immunofluorescence microscopy of myoblasts, isolated muscle fibres and skeletal muscle cryo-sections

Myoblasts were fixed in formaldehyde solution prepared from 4% of paraformaldehyde in PBS, permeabilized with 0.1% of Triton X-100 and immunostained as described [22]. Soleus muscle fibres and cryostat sections of 5 μ m thickness were prepared according to

[23,24] and [14], respectively, and processed for immunostaining using the Mouse on Mouse (M.O.M.) Basic Kit (Vector Laboratories, Burlingame, California, USA) as described in detail in [25]. Microscopy was performed using a LSM780 fluorescence laser scanning microscope (Carl Zeiss, Jena, Germany) equipped with a Plan-Apochromat 63× 1.4NA objective lens.

Immunofluorescence microscopy of skeletal muscle paraffin-sections

Samples from stretched soleus muscles were fixed in formaldehyde solution prepared from 4% of paraformaldehyde and 15% of saturated picric acid in PBS overnight at 4°C, dehydrated via ascending ethanol series, and embedded in paraffin. Sections of 5 µm were prepared with a RM 2235 microtome (Leica, Mannheim, Germany), rehydrated and blocked in peroxidase blocking buffer. A citrate-EGTA antigen recovery protocol was performed [20], slides were rinsed with PBS and blocked with 5% of bovine serum albumin containing 0.5% of Triton X-100 for 60 min. Subsequently, sections were incubated with primary and secondary antibodies each overnight at 4°C; stained samples were embedded in Mowiol supplemented with *N*-propyl-gallate (#02370; Sigma-Aldrich) to reduce photobleaching and analysed by confocal laser scanning microscopy (Eclipse Ti; Nikon, Minato, Tokio, Japan) using a 63× oil Plan-Apochromat objective.

Analysis of proteasomal activity

The trypsin-like proteasomal activity of soleus muscles was determined as described in detail in [26].

Ultrastructural analysis

Transmission electron microscopy was performed as described in [27]. Briefly, soleus muscle samples were fixed in fixation buffer (4% of paraformaldehyde, 15% of saturated picric acid and 0.5% of glutaraldehyde in 0.1 M phosphate buffer pH 7.4) overnight at 4°C. After rinsing in PBS, sections were treated with 0.5% of OsO₄, washed and counterstained with uranyl acetate, dehydrated via ethanol series and embedded in Durcupan resin (Fluka/Sigma-Aldrich). Ultrathin sections were prepared (Ultracut S; Leica) and examined with a Zeiss LEO

906E or Zeiss LEO 910 electron microscope (Carl Zeiss GmbH, Oberkochen, Germany).

Immunoelectron microscopy

Formaldehyde (4% of paraformaldehyde in PBS) fixed soleus muscle samples were cut into longitudinal 50 µm thick sections using a VT 1000S vibratome (Leica), rinsed twice in PBS, blocked for 1 h in 20% of normal goat serum, and incubated overnight at 4°C with primary antibodies diluted in PBS supplemented with 5% of normal goat serum. The sections were then triple-washed with PBS and incubated overnight at 4°C with 1.4 nm gold-coupled secondary antibodies (Nanoprobes, Yaphank, New York, USA). After extensive washing, sections were post-fixed in 1% of glutaraldehyde for 10 min and, after rinsing, sections reacted with the HQ Silver kit (Nanoprobes). After treatment with OsO₄, samples were counterstained with uranyl acetate in 70% of ethanol, dehydrated and embedded in Durcupan resin (Fluka/Sigma-Aldrich). Ultrathin sections were prepared from resin blocks with an Ultracut R device (Leica) and adsorbed on glow-discharged Formvar-carbon-coated copper grids. Microscopy was performed on a LEO 910 electron microscope (Carl Zeiss GmbH).

Data analysis and figure preparation

Data analysis and statistical evaluation were performed using Excel 2016 (Microsoft, Redmond, Washington, USA); the number of experiments is indicated in the figure legends; data are given as mean ± SEM; *P*-values were calculated by Student's *t*-test (heterozygous vs. wild-type or homozygous vs. wild-type values) and are **P*<0.05, ***P*<0.01, and ****P*<0.001, if not indicated otherwise. Final assembly and preparation of all figures for publication was done using Corel Draw Graphics Suite X7 (Corel, Austin, Texas, USA).

Results

From R349P desmin knock-in mice to an immortalized myoblast culture model for desminopathies

To establish a disease-mimicking muscle cell model for desminopathies, we cross-bred our previously reported

R349P desmin knock-in mouse line (B6J.129Sv-Des^{tm1.1Ccrs}) [14] with p53 knock-out mice (B6.129S2-Trp53^{tm1Tyj}) [15]. The rationale for this approach was that the targeted knock-out of the tumour suppressor p53 is an experimental strategy to overcome the Hayflick limit of primary myoblasts. Freshly prepared gastrocnemius and soleus muscles from offspring with the following three genotypes, homozygous R349P desmin knock-in/homozygous p53 knock-out, heterozygous R349P desmin knock-in/homozygous p53 knock-out and wild-type desmin/homozygous p53 knock-out were used for the generation of myoblast cultures, which subsequently underwent purification from fibroblasts (Figure 1A). Immunoblot analysis of total protein extracts derived from myoblast cultures that were differentiated into myotubes displayed desmin expression levels corresponding to the ones observed in skeletal muscle tissue from the desminopathy mice, including drastically reduced amounts of desmin protein in the homozygous R349P desmin knock-in samples (Figure 1B,D). Furthermore, immunostains revealed incomplete α -actinin and absent desmin cross-striated patterns in homozygous differentiated myotubes as compared to both wild-type and heterozygous cells (Figure 1C). Similarly, isolated skeletal muscle fibres in the homozygous R349P desmin knock-in mice showed an out-of-register α -actinin signal and the absence of the desmin cross-striation pattern (Figure 1E). Both, homozygous myotubes and isolated fibres displayed markedly reduced desmin protein levels and the presence of small, desmin-positive protein aggregates (Figure 1C,E).

Mutant desmin and the proteasome

To characterize the state of the protein quality control systems in response to the presence of R349P mutant desmin, we first analysed the trypsin-like proteasomal activity in soleus muscle lysates derived from heterozygous and homozygous mice as well as wild-type siblings. This analysis revealed 1.23-fold and 1.47-fold increases in hetero- and homozygous R349P desmin knock-in samples, respectively (Figure 2A). In keeping with an increased proteasomal activity in both desminopathy genotypes, analysis of the ubiquitination pattern showed decreased amounts of ubiquitinated proteins in muscle lysates from hetero- and homozygous mice (Figure 2B). To address the issue whether wild-type or R349P mutant desmin protein levels are influenced by the activity of the proteasome, we applied our newly generated immortalized myoblast model by treating myoblasts overnight with 10 μ M of the proteasome inhibitor MG132. Here, desmin immunoblotting revealed no obvious differences between MG132- and mock-treated myotubes (Figure 2C).

Mutant desmin and the autophagic system

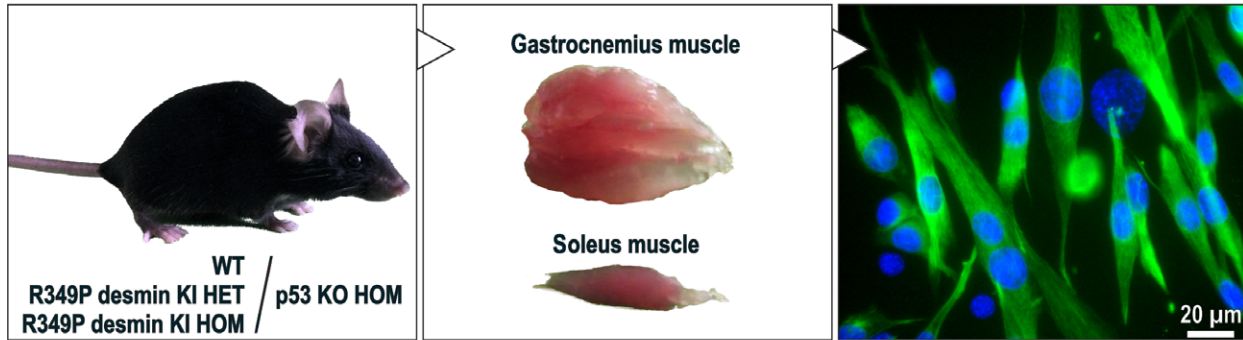
In a second step, we focused on the autophagic system in skeletal muscle tissue and differentiated myotubes derived from our desminopathy disease models. Cryosections of soleus muscles derived from hetero- and homozygous R349P desmin knock-in mice and wild-type sibling were double-immunolabelled using

Figure 1. From R349P desmin knock-in mice to an immortalized myoblast culture model for desminopathies. (A) Schematic drawing depicting the p53 knock-out mediated generation of immortalized myoblast cultures (desmin intermediate filament network in green, nuclei in blue) derived from gastrocnemius and soleus muscles of heterozygous and homozygous R349P desmin knock-in mice as well as wild-type littermates. (B) Expression of wild-type and R349P mutant desmin protein in 10 day differentiated myotubes of all three genotypes. The upper lane depicts the level of total desmin protein, whereas the middle lane solely visualizes the signal of the R349P mutant using a mutation-specific antibody [14]. Note the markedly decreased amount of desmin in the homozygous condition. GAPDH, loading control. (C) α -actinin (red) and desmin (green) immunostains of 10 day differentiated wild-type, heterozygous and homozygous R349P desmin knock-in myotubes. The pictures illustrate desmin intermediate filament networks that had not reached their full maturation as depicted by the lack of any clear cross-striation pattern. Note the markedly reduced desmin protein level and presence of small, desmin-positive protein aggregates in the homozygous cells as well as the absence of a cross-striated pattern in the α -actinin immunostain. (D) Expression of wild-type and R349P mutant desmin protein in skeletal muscle tissue from heterozygous and homozygous R349P desmin knock-in mice as well as wild-type littermates. Protein levels of total and R349P desmin protein as in (B). (E) α -actinin and desmin immunostains of isolated, teased muscle fibres derived from soleus muscles from desminopathy mice of all three genotypes. Note the out-of-register α -actinin signal pattern in homozygous fibres indicating severe disturbances in the lateral alignment of neighbouring myofibrils (arrowheads). The desmin stain denotes the markedly reduced desmin protein level, the absence of a regular cross-striation pattern and the presence of desmin-positive protein aggregates.

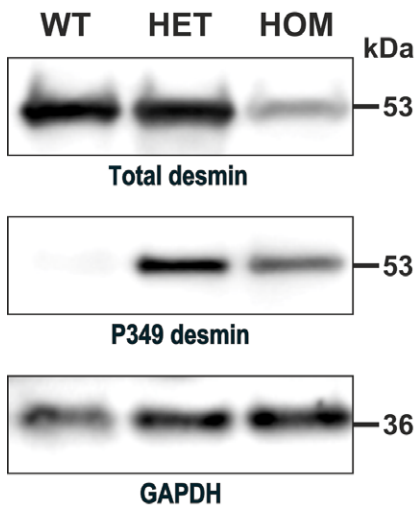
antibodies directed against desmin and the microtubule-associated protein LC3B. Here, wild-type and heterozygous specimens displayed virtually no LC3B

immunoreactivity, whereas multiple muscle fibres from homozygous mice showed small foci or larger sarcoplasmic areas with LC3B reactivity. However, only a

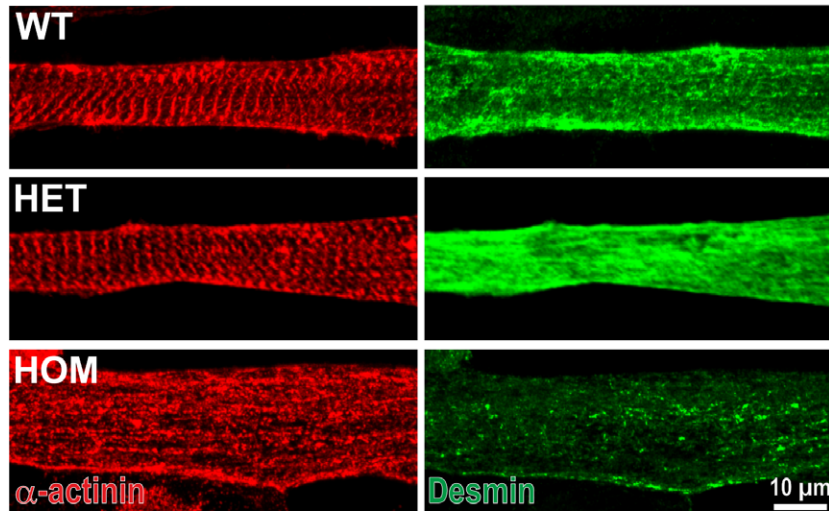
(A) p53 knock-out mediated generation of immortalized R349P desminopathy myoblasts



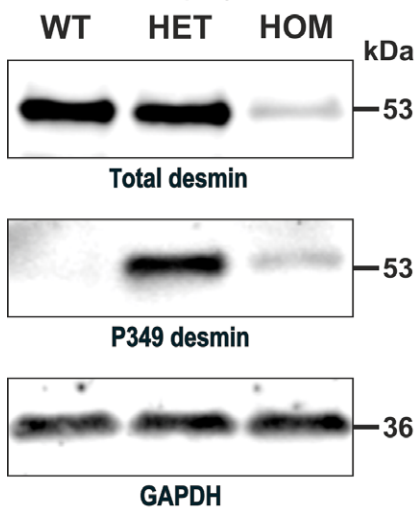
(B) R349P desminopathy myotubes



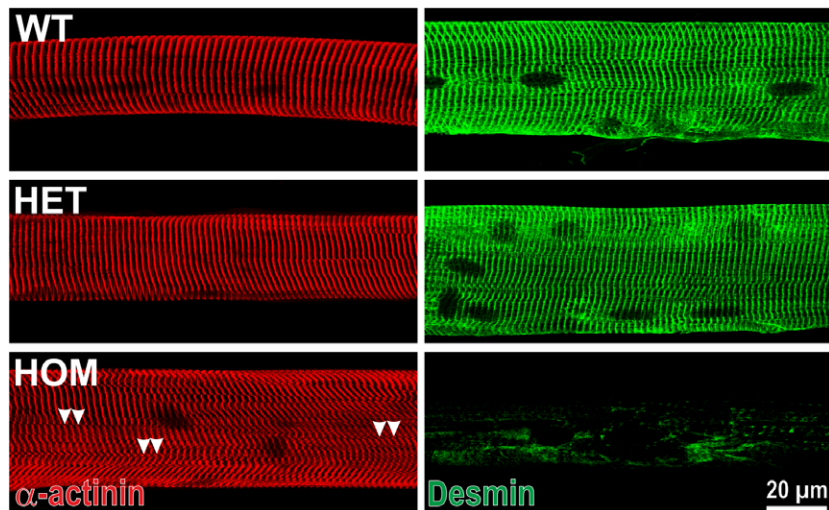
(C) R349P desminopathy myotubes



(D) R349P desminopathy soleus muscle



(E) R349P desminopathy isolated soleus muscle fibers



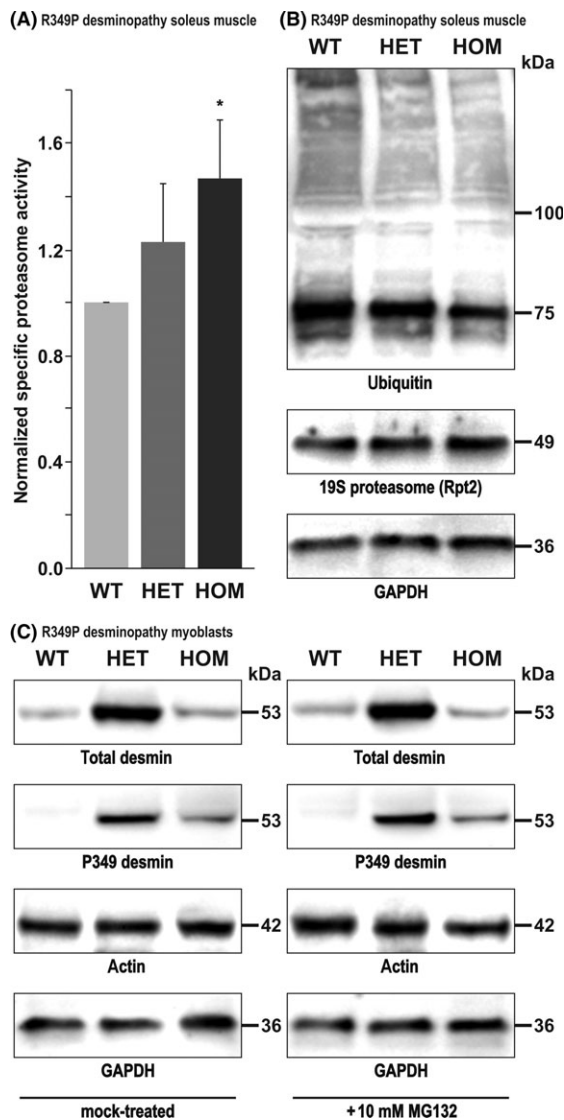


Figure 2. Proteasomal activity, ubiquitination pattern and the effect of proteasomal inhibition on wild-type and mutant desmin protein levels. (A) In comparison to wild-type soleus muscle (set to 1), hetero- as well as homozygous tissue samples showed an increase of the relative trypsin-like proteasomal activity. Muscles from two animals per genotype were analysed in six different experiments out of which ten values per genotype were obtained. (B) Ubiquitination pattern of equal amounts of total protein extracts from soleus muscles of heterozygous and homozygous R349P desmin knock-in mice as well as wild-type littermates. Note the overall decreased signal intensity of ubiquitinated proteins in hetero- and homozygous samples. 19S proteasome subunit 4 and GAPDH immunoblotting for control. (C) Effect of MG132 proteasome inhibition on the levels of wild-type and mutant desmin in cultured myoblasts. Though five independent experiments resulted in a stronger signal of the desmin band in heterozygous cells, the main finding is that MG132 treatment did not lead to any significant change in the amount of desmin in MG132 treated vs. non-treated myoblasts. Actin and GAPDH, loading controls.

small proportion of these LC3B-positive foci and sarcoplasmic areas also stained positive for desmin (Figure 3A). On the ultrastructural level, multiple small and large autophagic vacuoles were present in multiple muscle fibres from the soleus muscle specimens derived from homozygous, but not in samples from heterozygous R349P desmin knock-in mice and wild-type siblings (Figure 3B). The electron microscopy findings were further corroborated on the biochemical level by markedly increased protein levels of the serine/threonine protein kinase ULK1 and SQSTM1/p62 in soleus muscle from homozygous R349P desmin knock-in mice (Figure 3C,D). Corresponding analyses of 10 day differentiated myotubes also showed an increased level of SQSTM1/p62 in both homozygous and heterozygous cells (Figure 3E,F). Furthermore, in both genotypes the band corresponding to LC3-II (lower band; autophagosome membrane-bound form) was markedly elevated (Figure 3E,G). Subsequently, we examined the protein levels of filamin-C and BAG-3, both of which are essential components of the CASA system [28], in soleus muscle tissue and 10 day differentiated myotubes derived from hetero- and homozygous R349P desmin knock-in mice as well as wild-type siblings. While the protein levels of filamin-C and BAG-3 were markedly increased only in homozygous soleus muscle tissue (Figure 4A,B), they were more abundant compared to wild-type in both hetero- and homozygous desminopathy myotubes (Figure 4C,D).

Mutant desmin and the heat shock response

To assess whether the levels of heat shock proteins are altered in our desmin mutant mice, skeletal muscle lysates from hetero- and homozygous mice as well as wild-type siblings were analysed by immunoblotting using antibodies directed against α B-crystallin (synonym: HspB5), Hsp27 (synonyms: Hsp25, HspB1) and Hsp90. While the levels of all three heat shock proteins were in similar ranges in wild-type and heterozygous animals, their signal intensities in homozygous animals were markedly higher (Figure 5A,B). Corresponding analyses in 10 day differentiated desminopathy myotubes also showed elevated protein levels of α B-crystallin and Hsp27 in both heterozygous and homozygous cells, but not of Hsp90, which remained unchanged as compared to wild-type cells (Figure 5C, D).

Translocation of heat shock proteins to the level of sarcomeric I-bands

We recently demonstrated that α B-crystallin, Hsp27 and Hsp90 associate with I-band titin in various forms of human myopathies with and without evidence of abnormal protein aggregation [20,29]. To address this issue in our desminopathy mouse model, we performed corresponding immunogold electron microscopic analyses in homozygous and immunofluorescence imaging analyses in hetero- and homozygous animals compared to wild-type littermates. In the wild-type, our ultrastructural analyses of α B-crystallin and Hsp27 immunogold labelling denoted a strong enrichment of both small heat shock proteins at Z-discs, whereas Hsp90 was predominantly present at the level of Z-I junctions (Figure 6, left column). In contrast, both small heat shock proteins in homozygous desmin mice were found to be present at the level of I-bands with no significant immunolabelling of Z-discs. Furthermore, although to a lesser extent, Hsp90 also showed a predominant localization to sarcomeric I-bands (Figure 6, middle and right columns). Double-immunofluorescence stains of the PEVK-titin epitope in conjunction with either α B-crystallin, Hsp27, or Hsp90 further confirmed the translocation of all three heat shock proteins to the level of sarcomeric I-bands, both in homozygous as well as heterozygous R349P desmin knock-in mice as compared to the wild-type (Figure 7).

Discussion

In the present study, we exploited our newly generated immortalized muscle cell models in conjunction with the corresponding mouse models for dominant and recessive desminopathies to analyse pivotal protein quality control processes in the presence of R349P mutant desmin.

Mutant desmin and the proteasome

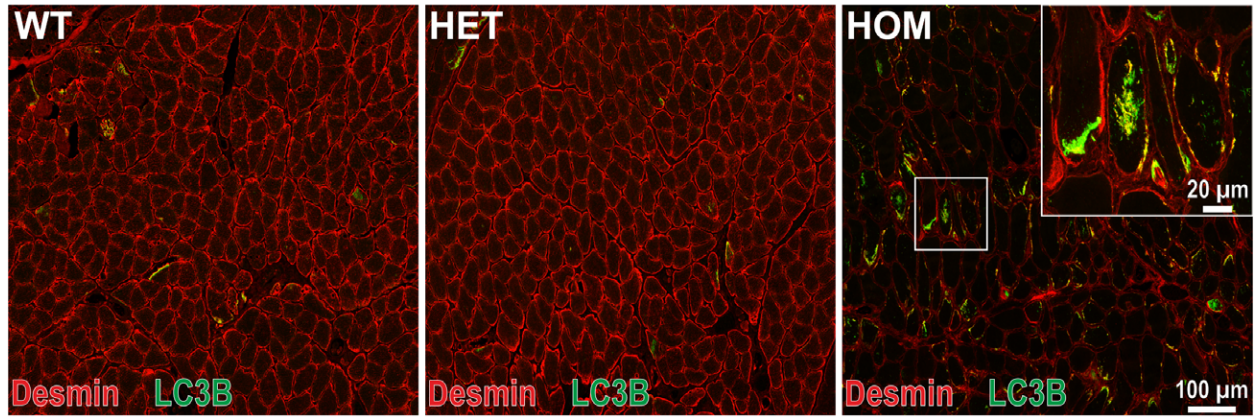
The proteasome hydrolyses intracellular proteins into small peptides, thus regulating protein turnover and removal of misfolded and poly-ubiquitinated proteins [30,31]. First, we analysed the trypsin-like proteasomal activity in skeletal muscle tissue, which revealed an increased enzymatic activity in heterozygous and

homozygous R349P desmin knock-in mice. Second, our analysis of the ubiquitination pattern in differentiated myotubes revealed decreased amounts of ubiquitinated proteins in both desminopathy genotypes. Third, upon MG132-mediated proteasome inhibition, the protein levels of R349P mutant and wild-type desmin remained constant. Thus, our results suggest that R349P mutant desmin increases the overall activity of the ubiquitin-proteasome system. However, our MG132 experiments did not provide evidence that wild-type or R349P mutant desmin levels are influenced by the abolished proteasomal activity. In contrast, a previous study reported that the overexpression of p.Arg173_Glu179del mutant desmin in cultured neonatal rat ventricular myocytes not only led to the formation of desmin-positive protein aggregates, but inhibited the function of the ubiquitin-proteasome system in a dose-dependent manner [32]. Another study in cardiac tissue of the transgenic *Des^{tg p.Arg173_Glu179del}* desminopathy mouse model [33], which had been crossed with a transgenic mouse model expressing the GFPdgn ubiquitin-proteasome system reporter substrate [34] resulting in *Des^{tg p.Arg173_Glu179del}/GFPdgn^{tg}* mice [35], reported that the overexpression of p.Arg173_Glu179del mutant desmin also increased the proteasomal activity; however, it also led to higher levels of ubiquitinated proteins. Here, the authors concluded that the entry of ubiquitinated proteins into the 20S core proteasome is compromised by the mutant desmin [35]. Other recent studies reported that the normal desmin cytoskeleton is ubiquitinated and disassembled by Trim32 followed by degradation involving the VCP/p97 ATPase [36], and that misfolded desmin prior to aggregate formation is recognized and guided to proteasomal degradation by the MTM1-UBQLN2 complex [37]. Since the individual study findings are directly influenced by the different types of myogenic cells and striated muscle tissues used, the respective mutation status – missense vs. deletion mutation vs. no mutation – as well as the different expression levels of the mutant desmin proteins (knock-in expression vs. transgenic overexpression), the divergent results cannot conclusively be reconciled at present.

Mutant desmin and the macroautophagy

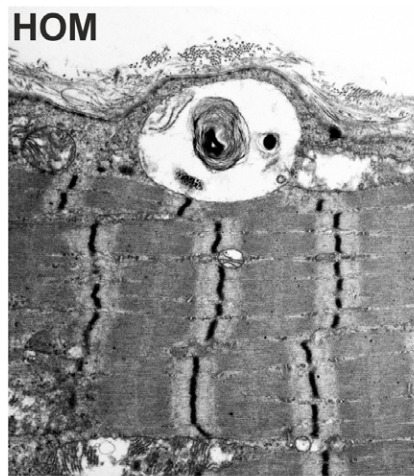
The second major cellular system for the removal of misfolded and poly-ubiquitinated proteins is the

(A) R349P desminopathy soleus muscle

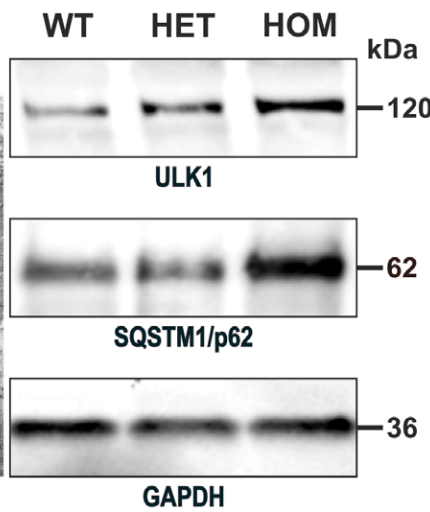


COLOR

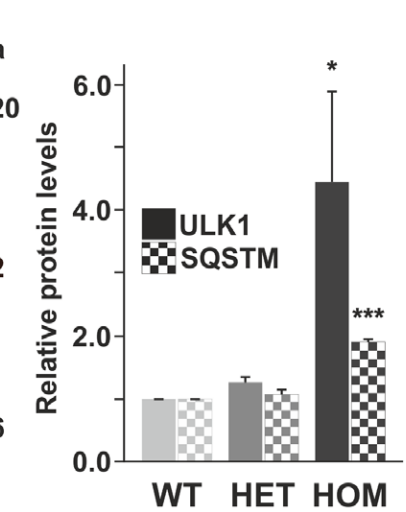
(B) R349P desminopathy soleus muscle



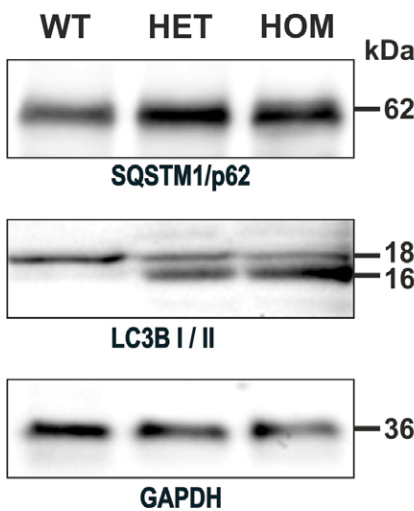
(C) R349P desminopathy soleus muscle



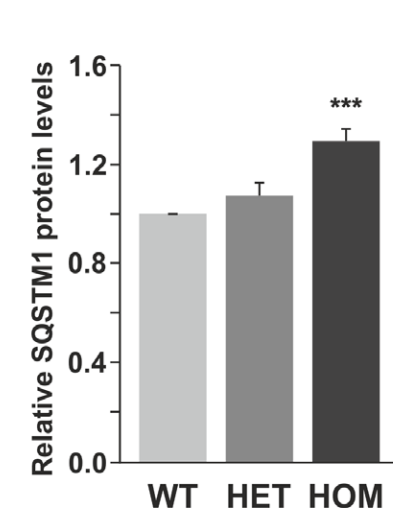
(D) R349P desminopathy soleus muscle



(E) R349P desminopathy myotubes



(F) R349P desminopathy myotubes



(G) R349P desminopathy myotubes

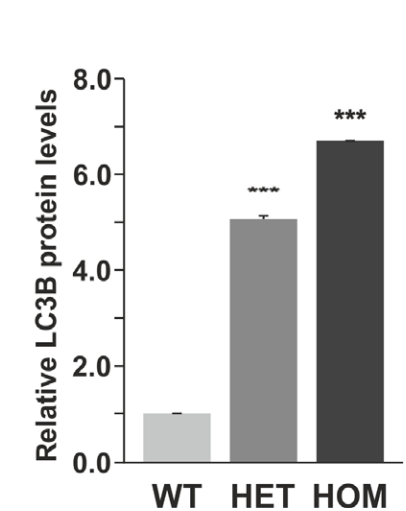


Figure 3. Effects of R349P mutant desmin on the autophagic system in skeletal muscle tissue and differentiated myotubes. (A) Double-immunostains of soleus muscles using antibodies directed against desmin (red) and light chain 3B (LC3B) (green). While wild-type and heterozygous specimens displayed virtually no LC3B immunoreactivity, multiple muscle fibres derived from homozygous mice showed small foci or larger sarcoplasmic areas with LC3B reactivity. (B) Electron micrograph depicting a classical autophagic vacuole containing a myelin-like body in the subsarcolemmal area of a homozygous R349P desmin knock-in muscle fibre. (C) Immunoblot addressing the amounts of the autophagy markers ULK1 and sequestosome 1 (SQSTM1)/p62, which are significantly increased in homozygous muscle tissue. GAPDH as loading control. (D) Densitometry analysis of the band intensities of ULK1 and SQSTM1/p62 immunoblots (three of each) normalized to the total protein content per line as determined by separate Coomassie brilliant blue stained gels (not shown). (E) SQSTM1/p62 and LC3B immunoblot analysis of differentiated myotubes of all three genotypes. Note the increased SQSTM1/p62 signal intensity and the presence of LC3B-II in hetero- and homozygous myotubes. GAPDH as loading control. (F) Densitometry analysis of SQSTM1/p62 band intensities from three different immunoblots normalized to the total protein content per line as determined by separate Coomassie brilliant blue stained gels (not shown). (G) Relative amounts of LC3B-II/LC3B-I based on the densitometry analysis of their respective signal intensities in three different immunoblots.

autophagy-lysosome system [38,39]. Our key findings in the analysis of macroautophagy were increased LC3B immunoreactivity, ultrastructural evidence of abundant autophagic vacuoles, and increased protein levels of the ULK1 initiator of and the SQSTM1/p62 receptor for autophagy [40] in skeletal muscle tissue derived from homozygous R349P desmin knock-in mice. Notably, the increased levels of SQSTM1/p62 and LC3B-II, the active membrane bound form of LC3B, were noted in differentiated heterozygous and homozygous R349P desmin knock-in myotubes. Experimental evidence for augmented macroautophagy in desminopathies was also provided by a study using the above mentioned *Des^{tg p.Arg173_Glu179del}* mouse strain cross-bred with a transgenic autophagy reporter mouse model expressing a GFP-LC3 fusion protein [41]. Here, expression of the desmin deletion mutant led to an increased autophagic flux associated with an increased expression of SQSTM1/p62 [42]. Even more important, several studies on human skeletal muscle from patients with different heterozygous desmin mutations described by means of light and electron microscopy displayed increased numbers of autophagic vacuoles, which are the morphological hallmark of an increased autophagic build-up [43–45]. Together, the overall findings in human biopsy specimens as well as in various desminopathy disease models clearly demonstrate that the presence of mutant desmin protein variants leads to an induction of macroautophagy.

Mutant desmin and the CASA

In striated muscle tissue, a specific form of autophagy, the so-called CASA, has an essential role in the degradation of damaged Z-disc structures [40,46,47]. Our

immunoblots showed markedly increased protein levels of BAG-3 and filamin-C in both desminopathy skeletal muscle tissue and differentiated myotubes. While these findings clearly indicate an aberrant regulation of the CASA machinery inflicted by the presence of R349P mutant desmin, the exact meaning of a combined increase of BAG-3 and filamin-C levels is currently unclear [47].

Mutant desmin and the heat shock response

α B-crystallin and Hsp27 belong to the family of small heat shock proteins and exert essential roles in protecting cells against various forms of stress including heat shock, oxidative, osmotic and mechanical stress. These multifunctional proteins recognize unfolded proteins and prevent their aggregation [48]. Previous analyses demonstrated that α B-crystallin and Hsp27 directly bind to desmin [49,50], and that both proteins are significantly accumulated in protein aggregates of striated muscle biopsy specimens from human desminopathy patients [1,45,51]. Recent work further showed that α B-crystallin serves as an assembly chaperone, which has a sensor function for the surface topology of desmin filaments forming from wild-type and mutated desmin [52].

Our immunoblot analysis showed increased levels of α B-crystallin and Hsp27 in skeletal muscle tissue derived from homozygous R349P desmin knock-in mice as well as in hetero- and homozygous desminopathy myotubes. Further, our immunogold electron and immunofluorescence microscopic analyses revealed that the increased levels of both heat shock proteins are coupled with distinct changes in their sarcomeric localization. While normal murine skeletal muscle displayed

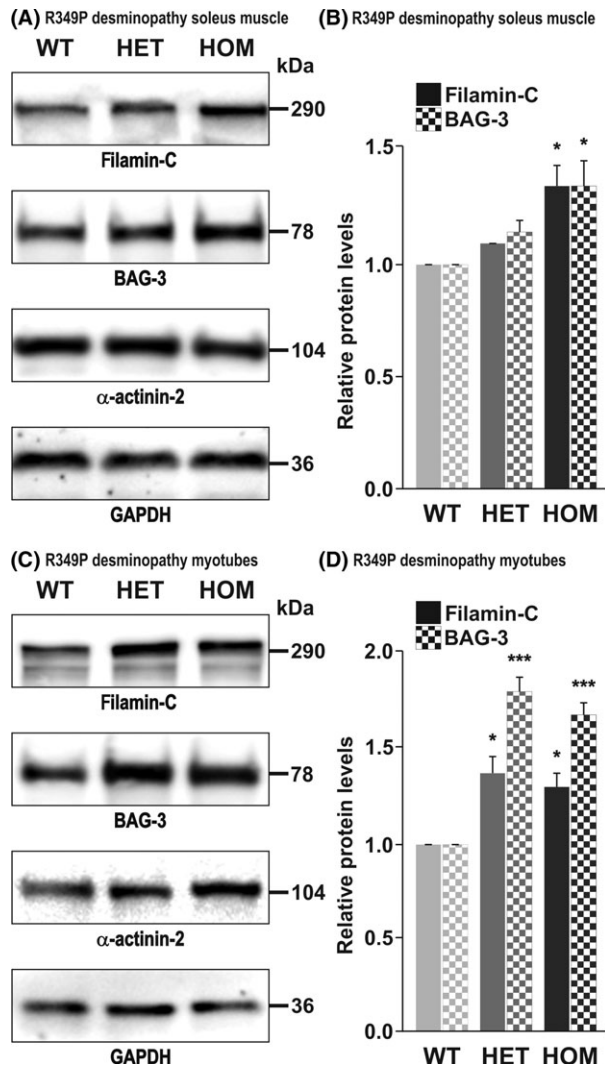


Figure 4. Expression profiles of the chaperone-assisted selective autophagy-related proteins filamin-C and BAG-3. Immunoblots addressing the levels of filamin-C and BAG-3 in R349P desmin knock-in muscle tissue (A) and differentiated myotubes (C). α -actinin and GAPDH as loading controls. (B and D) Corresponding densitometry analysis of the band intensities from seven (filamin-C) and four (BAG-3) different immunoblots of each expression analysis normalized to the total protein content per line as determined by separate Coomassie brilliant blue stained gels (not shown). Note the significantly increased levels of filamin-C and BAG-3 in both settings.

a strong enrichment of α B-crystallin and Hsp27 at Z-discs, they both were predominantly present at the level of I-bands in close proximity to the PEVK-titin epitope in skeletal muscle of hetero- and homozygous R349P desmin knock-in mice. Beyond a crucial role in the organization of the three-dimensional desmin

intermediate filament cytoskeleton itself, our findings further highlight the notion that α B-crystallin and Hsp27 display aberrant sarcomeric localization pattern in stressed as well as diseased striated muscle that clearly differs from the ones observed in normal skeletal muscle. Similar to the results observed in our desminopathy mouse models, analyses of adult zebrafish myocardium exposed to hyperthermia and mechanical stretching [53] as well as of human skeletal muscle samples derived from patients with myopathies with or without evidence of abnormal protein aggregation [20,29] revealed a translocation of both small heat shock proteins from a localization at Z-bands to the level I-band titin.

We also observed a sarcomeric translocation of the ATP-dependent chaperone Hsp90, which modulates myofibril organization and myosin assembly [54–58], from the level of Z-I junctions to sarcomeric I-bands in the murine desminopathy skeletal muscle tissue. Thus, our findings complement previously published work, which showed an identical translocation of Hsp90 in diseased human and murine skeletal muscle tissue [20]. Methylation of Hsp90 by the methyltransferase Smyd2 results in the binding of Hsp90 to the N2A element of I-band titin, which has been implicated to have a stabilizing effect on the myofibrillar Z-disc/I-band structure [59,60].

The increased levels of α B-crystallin and Hsp27 along with the observed myofibrillar translocation of all three heat shock proteins strongly indicate that these molecular chaperones exert a critical role in protecting and stabilizing the myofibrillar Z-disc/I-band structure in mechanically stressed [61] and diseased [20] striated muscle tissue. Notably, recent studies reported that sarcomere stretching leads to the unfolding of previously concealed hydrophobic titin Ig domains in the I-band [62]. Since α B-crystallin and Hsp27 preferentially bind to these elastic titin springs in I-bands [29], it was postulated that this binding may lower the risk of irreversible aggregation of this particular sarcomere structure. Beyond mere pathophysiological significance, this notion is also of interest in defining novel therapeutic concepts for desminopathies and other forms of protein aggregate myopathies. In this context, it is noteworthy that the pharmacological induction of Hsp27 protein levels by geranylgeranylacetone [63], the overexpression of α B-crystallin [32] as well as the drug treatment with the chemical chaperone 4-

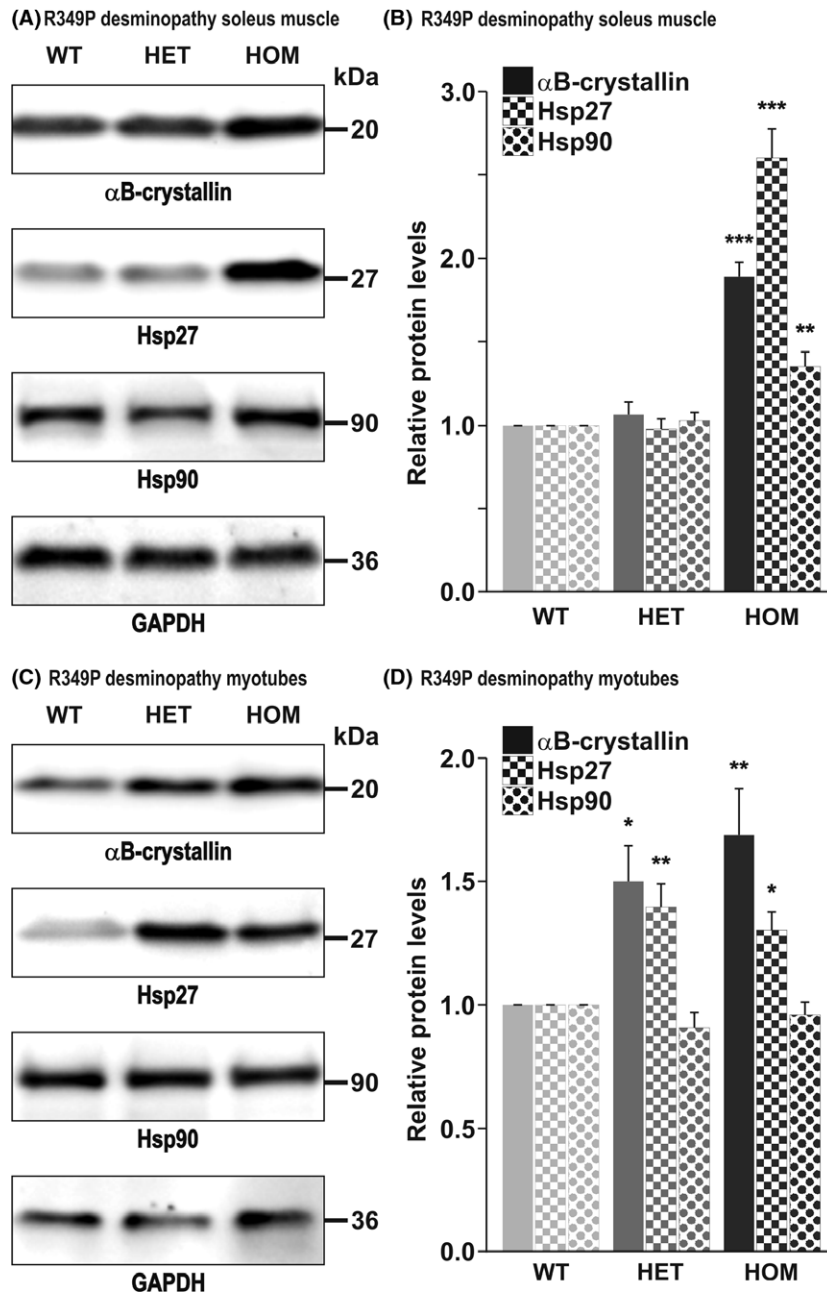


Figure 5. Expression profiles of heat shock proteins. Immunoblots addressing the levels of the small heat shock proteins α B-crystallin and Hsp27 as well as Hsp90 in R349P desmin knock-in muscle tissue (A) and differentiated myotubes (C). GAPDH as loading control. (B and D) Corresponding densitometry analysis of the band intensities from three different immunoblots of each expression analysis normalized to the total protein content per line as determined by separate Coomassie brilliant blue stained gels (not shown). Note the increased and seemingly unchanged levels of all three heat shock proteins in homozygous and heterozygous muscle tissue, respectively. The pattern in myotubes is more complex; here, α B-crystallin is upregulated in both genotypes, Hsp27 only in the homozygous condition, and Hsp90 shows no regulation.

phenylbutyric acid [17], all resulted in a reduction of desmin protein aggregation pathology and in an improvement of the striated muscle morphology and function in disease models for α B-crystallinopathies,

desminopathies and plectinopathies [17,32,64]. While the positive treatment effects on the protein aggregation pathology may primarily be attributed to the chaperone activities of α B-crystallin and Hsp27 on the

R349P desminopathy soleus muscle

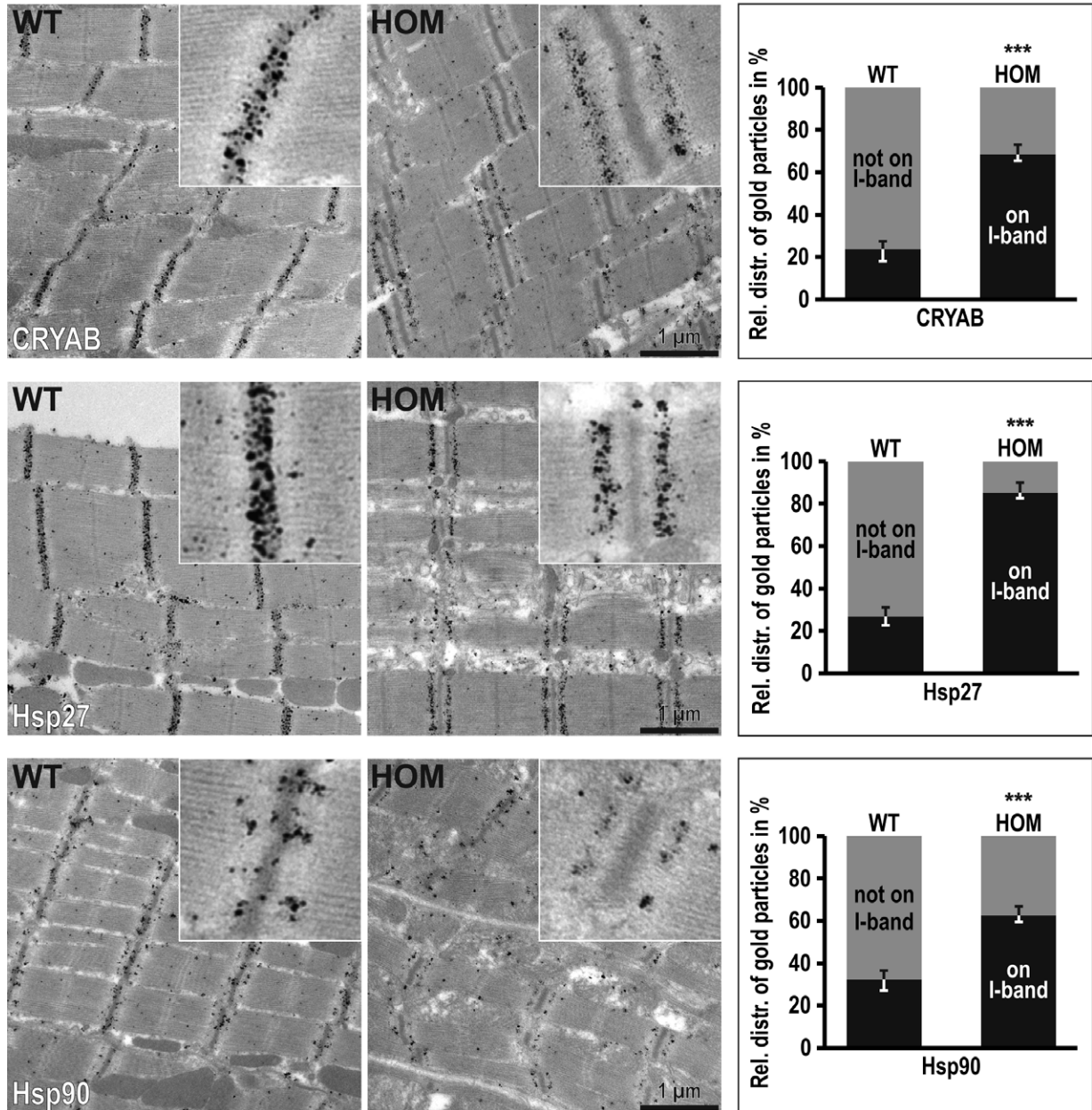


Figure 6. Immunogold localization of heat shock proteins. (Left and middle column) Nanogold-labelled immunoelectron micrographs and higher-power magnification insets depicting the sarcomeric localization of α B-crystallin, Hsp27 and Hsp90 in skeletal muscle tissue derived from homozygous R349P desmin knock-in mice and wild-type littermates. (Right column) Quantitation of the nanogold particle distribution. The number of gold particles was counted in 40 different $30 \mu\text{m}^2$ -sized regions-of-interest from two muscle specimens derived from two animals per genotype. The stacked column charts indicate the relative distribution of gold particles in percent on the level of sarcomeric I-bands (I-band) or elsewhere in the sarcomeric region (not I-band). α B-crystallin (values homozygote vs. wild-type): total number of gold particles, 2712 vs. 938; mean number on I-band, 47 vs. 6; mean number not on I-band, 21 vs. 18; statistical significance, $P = 3 \times 10^{-20}$. Hsp27 (values homozygote vs. wild-type): total number of gold particles, 2609 vs. 1091; mean number on I-band, 56 vs. 7; mean number not on I-band, 10 vs. 20; statistical significance, $P = 4 \times 10^{-37}$. Hsp90 (values homozygote vs. wild-type): total number of gold particles, 1678 vs. 1331; mean number on I-band, 26 vs. 11; mean number not on I-band, 16 vs. 23; statistical significance, $P = 7 \times 10^{-13}$. Note the strong enrichment of α B-crystallin and Hsp27 at Z-discs in normal skeletal muscle and their prominent translocation to sarcomeric I-bands in homozygous desminopathy mice. Moreover, Hsp90, which predominantly localized at the level of Z-I junctions in normal muscle, also shows a relocalization to sarcomeric I-bands.

R349P desminopathy soleus muscle

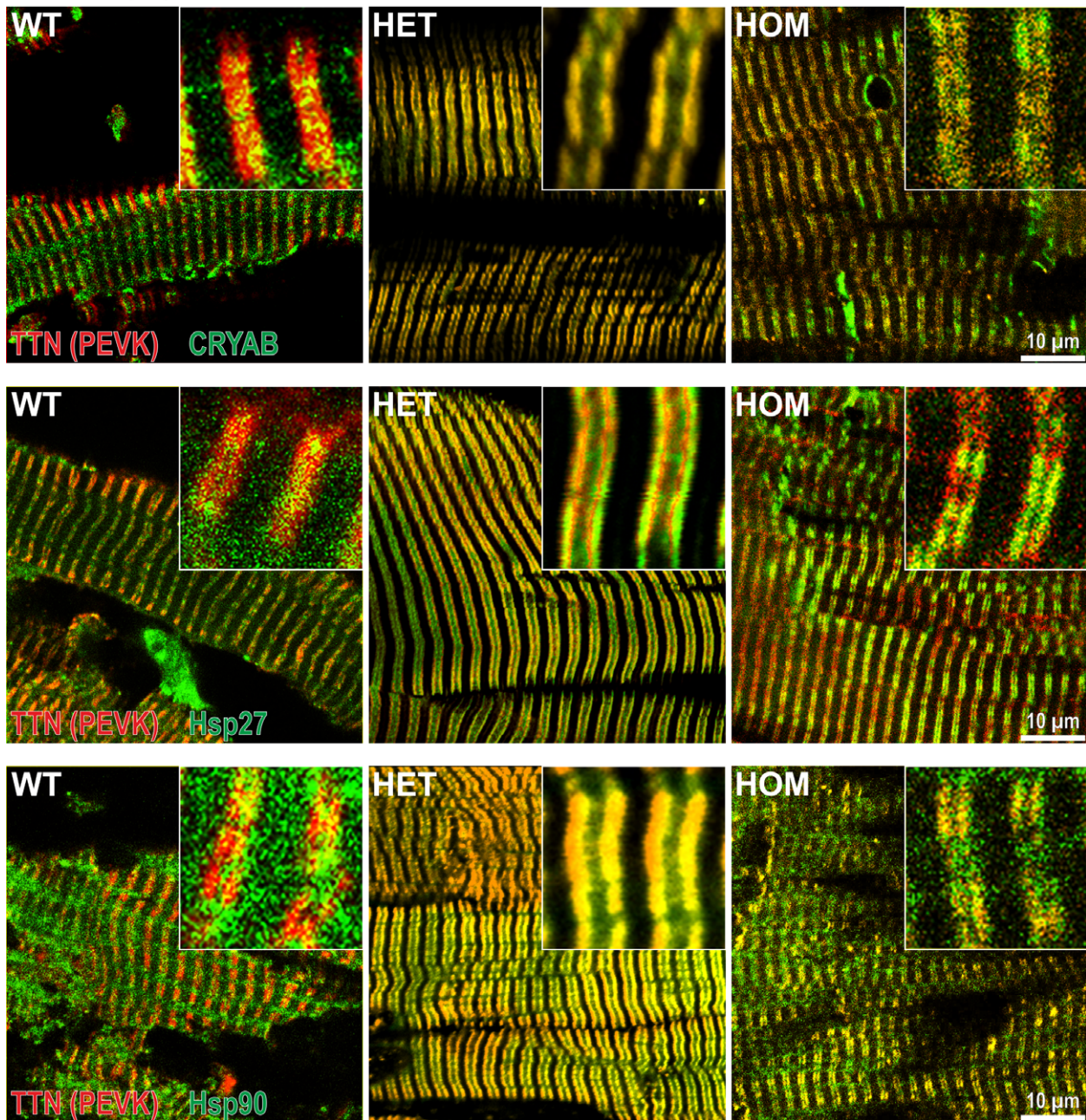


Figure 7. Immunofluorescence analysis of heat shock proteins. Double-immunofluorescence stains in soleus muscle tissue derived from heterozygous and homozygous R349P desmin knock-in mice as well as wild-type littermates using antibodies directed against the PEVK-titin epitope (in red) and either α B-crystallin, Hsp27 or Hsp90 (each in green). Note that the translocation of all three heat shock proteins to the level of sarcomeric I-bands closely mirrors the immunogold results.

desmin filament system, it is tempting to speculate that the functional improvement, i.e. the increased muscle strength, may result from the here reported sarcomeric translocation of both small heat shock proteins. This

hypothesis is further supported by another study showing that exogenous α B-crystallin reduced desmin and titin degradations in myofibrillar extracts and attenuated μ -calpain (calpain-1 catalytic subunit and calpain

small regulatory subunit 1) activity, which is implicated in the cleavage and degradation of the three-dimensional desmin intermediate filament system [65]. Thus, the markedly increased levels of both small heat shock proteins in desminopathies and other forms of protein aggregate myopathies are likely to reflect a heightened demand of these two molecular chaperones, both in the desmin intermediate filament as well as in the myofibrillar compartments.

In conclusion, our data revealed that R349P mutant desmin causes a general imbalance in all major protein quality control systems. The increased activity of these systems in conjunction with the sarcomeric translocation of heat shock proteins may be responsible for the previously observed increased turnover of desmin as well as desmin-binding partners [14], which triggers progressive dysfunction of the extrasarcomeric cytoskeleton and the myofibrillar apparatus in autosomal-dominant and autosomal-recessive desminopathies with maintained desmin protein expression. Furthermore, our newly generated desminopathy cell model provides a basis for further pathophysiological as well as pharmacological and genetic intervention studies.

Acknowledgements

LW was supported by the ELAN Program of the Friedrich-Alexander University Erlangen-Nuremberg (13-04-28-1-Winter). IW was supported by the German Research Foundation (DFG) (SFB815, project Z01). CSC and RS were supported by the DFG within the framework of the multi-location research group FOR1228 (CL 381/7-1 to CSC and SCHR 562/13-1 to RS). RS and CSC were supported by the German Muscular Dystrophy Network (MD-NET2) funded by the German Ministry of Education and Research (BMBF) (project 7), and by the Deutsche Gesellschaft für Muskelkranke e.V. (DGM). We thank Dieter O. Fürst (University of Bonn, Germany) for providing a filamin-C antibody. We thank Dorothea Schultheis and Harald Herrmann (University Hospital Erlangen, Germany) for critically reading the manuscript.

Author contributions

LW, CSC and RS jointly conceived the study, reviewed all data, prepared the figures, and wrote the manuscript. LW, AU, FC, KHS, IW and CSC designed and

carried out experiments and analysed data. CB, MS, MW and MT carried out experiments and analysed data. USS, WHG, KM and WAL designed experiments and analysed data. All authors read and approved the final version of manuscript text and figures.

Conflict of interest

The authors declare that they have no conflict of interest.

References

- 1 Clemen CS, Herrmann H, Strelkov SV, Schröder R. Desminopathies: pathology and mechanisms. *Acta Neuropathol* 2013; **125**: 47–75
- 2 Diermeier S, Buttgereit A, Schuermann S, Winter L, Xu H, Murphy RM, Clemen CS, Schroeder R, Friedrich O. Preaged remodeling of myofibrillar cytoarchitecture in skeletal muscle expressing R349P mutant desmin. *Neurobiol Aging* 2017; **58**: 77–87
- 3 Diermeier S, Iberl J, Vetter K, Haug M, Pollmann C, Reischl B, Buttgereit A, Schürmann S, Spörrer M, Goldmann WH, Fabry B. Early signs of architectural and biomechanical failure in isolated myofibers and immortalized myoblasts from desmin-mutant knock-in mice. *Sci Rep* 2017; **7**: 1391
- 4 Palmisano MG, Bremner SN, Hornberger TA, Meyer GA, Domenighetti AA, Shah SB, Kiss B, Kellermayer M, Ryan AF, Lieber RL. Skeletal muscle intermediate filaments form a stress-transmitting and stress-signaling network. *J Cell Sci* 2015; **128**: 219–24
- 5 Goldfarb LG, Park KY, Cervenáková L, Gorokhova S, Lee HS, Vasconcelos O, Nagle JW, Semino-Mora C, Sivakumar K, Dalakas MC. Missense mutations in desmin associated with familial cardiac and skeletal myopathy. *Nat Genet* 1998; **19**: 402–3
- 6 Muñoz-Mármol AM, Strasser G, Isamat M, Coulombe PA, Yang Y, Roca X, Vela E, Mate JL, Coll J, Fernández-Figueras MT, Navas-Palacios JJ. A dysfunctional desmin mutation in a patient with severe generalized myopathy. *Proc Natl Acad Sci U S A* 1998; **95**: 11312–17
- 7 Piñol-Ripoll G, Shatunov A, Cabello A, Larrodé P, de la Puerta I, Pelegrín J, Ramos FJ, Olivé M, Goldfarb LG. Severe infantile-onset cardiomyopathy associated with a homozygous deletion in desmin. *Neuromuscul Disord* 2009; **19**: 418–22
- 8 Arbustini E, Morbini P, Grasso M, Fasani R, Verga L, Bellini O, Dal Bello B, Campana C, Piccolo G, Febo O, Opasich C. Restrictive cardiomyopathy, atrioventricular block and mild to subclinical myopathy in patients with desmin-immunoreactive material deposits. *J Am Coll Cardiol* 1998; **31**: 645–53

- 9 Cetin N, Balci-Hayta B, Gundesli H, Korkusuz P, Purali N, Talim B, Tan E, Selcen D, Erdem-Ozdamar S, Dincer P. A novel desmin mutation leading to autosomal recessive limb-girdle muscular dystrophy: distinct histopathological outcomes compared with desminopathies. *J Med Genet* 2013; **50**: 437–43
- 10 Henderson M, De Waele L, Hudson J, Eagle M, Sewry C, Marsh J, Charlton R, He L, Blakely EL, Horrocks I, Stewart W. Recessive desmin-null muscular dystrophy with central nuclei and mitochondrial abnormalities. *Acta Neuropathol* 2013; **125**: 917–19
- 11 Carmignac V, Sharma S, Arbogast S, Fischer D, Serreri C, Serria M, Stoltenburg G, Maurage CA, Herrmann H, Cuisset JM, Bär H. A homozygous desmin deletion causes an Emery-Dreifuss like recessive myopathy with desmin depletion. *Neuromuscul Disord* 2009; **19**: 600
- 12 McLaughlin HM, Kelly MA, Hawley PP, Darras BT, Funke B, Picker J. Compound heterozygosity of predicted loss-of-function DES variants in a family with recessive desminopathy. *BMC Med Genet* 2013; **14**: 68
- 13 Durmuş H, Ayhan Ö, Çırak S, Deymeer F, Parman Y, Franke A, Eiber N, Chevessier F, Schlötzer-Schrehardt U, Clemen CS, Hashemolhosseini S. Neuromuscular endplate pathology in recessive desminopathies: lessons from man and mice. *Neurology* 2016; **87**: 799–805
- 14 Clemen CS, Stöckigt F, Strucksberg KH, Chevessier F, Winter L, Schütz J, Bauer R, Thorweihe JM, Wenzel D, Schlötzer-Schrehardt U, Rasche V. The toxic effect of R350P mutant desmin in striated muscle of man and mouse. *Acta Neuropathol* 2015; **129**: 297–315
- 15 Jacks T, Remington L, Williams BO, Schmitt EM, Halachmi S, Bronson RT, Weinberg RA. Tumor spectrum analysis in p53-mutant mice. *Curr Biol* 1994; **4**: 1–7
- 16 Metz T, Harris AW, Adams JM. Absence of p53 allows direct immortalization of hematopoietic cells by the myc and raf oncogenes. *Cell* 1995; **82**: 29–36
- 17 Winter L, Staszewska I, Mihailovska E, Fischer I, Goldmann WH, Schröder R, Wiche G. Chemical chaperone ameliorates pathological protein aggregation in plectin-deficient muscle. *J Clin Invest* 2014; **124**: 1144–57
- 18 Rosenblatt JD, Lunt AI, Parry DJ, Partridge TA. Culturing satellite cells from living single muscle fiber explants. *In Vitro Cell Dev Biol Anim* 1995; **31**: 773–9
- 19 Kley RA, Maerkens A, Leber Y, Theis V, Schreiner A, van der Ven PF, Uszkoreit J, Stephan C, Eulitz S, Euler N, Kirschner J. A combined laser microdissection and mass spectrometry approach reveals new disease relevant proteins accumulating in aggregates of filaminopathy patients. *Mol Cell Proteomics* 2013; **12**: 215–27
- 20 Unger A, Beckendorf L, Böhme P, Kley R, von Frieling-Salewsky M, Lochmüller H, Schröder R, Fürst DO, Vorgerd M, Linke WA. Translocation of molecular chaperones to the titin springs is common in skeletal myopathy patients and affects sarcomere function. *Acta Neuropathol Commun* 2017; **5**: 72
- 21 Chopard A, Pons F, Charpiot P, Marini JF. Quantitative analysis of relative protein contents by Western blotting: comparison of three members of the dystrophin-glycoprotein complex in slow and fast rat skeletal muscle. *Electrophoresis* 2000; **21**: 517–22
- 22 Winter L, Abrahamsberg C, Wiche G. Plectin isoform 1b mediates mitochondrion-intermediate filament network linkage and controls organelle shape. *J Cell Biol* 2008; **181**: 903–11
- 23 Konieczny P, Fuchs P, Reipert S, Kunz WS, Zeöld A, Fischer I, Paulin D, Schröder R, Wiche G. Myofiber integrity depends on desmin network targeting to Z-disks and costameres via distinct plectin isoforms. *J Cell Biol* 2008; **181**: 667–81
- 24 Rezniczek GA, Konieczny P, Nikolic B, Reipert S, Schneller D, Abrahamsberg C, Davies KE, Winder SJ, Wiche G. Plectin 1f scaffolding at the sarcolemma of dystrophic (mdx) muscle fibers through multiple interactions with beta-dystroglycan. *J Cell Biol* 2007; **176**: 965–77
- 25 Winter L, Wittig I, Peeva V, Eggers B, Heidler J, Chevessier F, Kley RA, Barkovits K, Strecker V, Berwanger C, Herrmann H. Mutant desmin substantially perturbs mitochondrial morphology, function and maintenance in skeletal muscle tissue. *Acta Neuropathol* 2016; **132**: 453–73
- 26 Strucksberg KH, Tangavelou K, Schröder R, Clemen CS. Proteasomal activity in skeletal muscle: a matter of assay design, muscle type, and age. *Anal Biochem* 2010; **399**: 225–9
- 27 Chevessier F, Schuld J, Orfanos Z, Plank AC, Wolf L, Maerkens A, Unger A, Schlötzer-Schrehardt U, Kley RA, Von Hörsten S, Marcus K. Myofibrillar instability exacerbated by acute exercise in filaminopathy. *Hum Mol Genet* 2015; **24**: 7207–20
- 28 Ulbricht A, Arndt V, Hohfeld J. Chaperone-assisted proteostasis is essential for mechanotransduction in mammalian cells. *Commun Integr Biol* 2013; **6**: e24925
- 29 Kötter S, Unger A, Hamdani N, Lang P, Vorgerd M, Nagel-Steger L, Linke WA. Human myocytes are protected from titin aggregation-induced stiffening by small heat shock proteins. *J Cell Biol* 2014; **204**: 187–202
- 30 Sorokin AV, Kim ER, Ovchinnikov LP. Proteasome system of protein degradation and processing. *Biochemistry* 2009; **74**: 1411–42
- 31 Jung T, Catalgol B, Grune T. The proteasomal system. *Mol Aspects Med* 2009; **30**: 191–296
- 32 Liu J, Tang M, Mestrlil R, Wang X. Aberrant protein aggregation is essential for a mutant desmin to impair the proteolytic function of the ubiquitin-proteasome system in cardiomyocytes. *J Mol Cell Cardiol* 2006; **40**: 451–4

- 33 Wang X, Osinska H, Dorn GW, Nieman M, Lorenz JN, Gerdes AM, Witt S, Kimball T, Gulick J, Robbins J. Mouse model of desmin-related cardiomyopathy. *Circulation* 2001; **103**: 2402–7
- 34 Kumarapeli AR, Horak KM, Glasford JW, Li J, Chen Q, Liu J, Zheng H, Wang X. A novel transgenic mouse model reveals deregulation of the ubiquitin-proteasome system in the heart by doxorubicin. *FASEB J* 2005; **19**: 2051–3
- 35 Liu J, Chen Q, Huang W, Horak KM, Zheng H, Mestril R, Wang X. Impairment of the ubiquitin-proteasome system in desminopathy mouse hearts. *FASEB J* 2006; **20**: 362–4
- 36 Volodin A, Kostic I, Goldberg AL, Cohen S. Myofibril breakdown during atrophy is a delayed response requiring the transcription factor PAX4 and desmin depolymerization. *Proc Natl Acad Sci U S A* 2017; **114**: E1375–84
- 37 Gavriilidis C, Laredj L, Solinhac R, Messaddeq N, Viaud J, Laporte J, Sumara I, Hnia K. The MTM1-UBQLN2-HSP complex mediates degradation of misfolded intermediate filaments in skeletal muscle. *Nat Cell Biol* 2018; **20**: 198–210
- 38 Cohen-Kaplan V, Livneh I, Avni N, Cohen-Rosenzweig C, Ciechanover A. The ubiquitin-proteasome system and autophagy: coordinated and independent activities. *Int J Biochem Cell Biol* 2016; **79**: 403–18
- 39 Yu S, Melia TJ. The coordination of membrane fission and fusion at the end of autophagosome maturation. *Curr Opin Cell Biol* 2017; **47**: 92–8
- 40 Klionsky DJ, Abdelmohsen K, Abe A, Abedin MJ, Abeliovich H, Acevedo Arozena A, Adachi H, Adams CM, Adams PD, Adeli K, Adhietty PJ. Guidelines for the use and interpretation of assays for monitoring autophagy. *Autophagy* 2016; **12**: 1–222
- 41 Mizushima N, Yamamoto A, Matsui M, Yoshimori T, Ohsumi Y. In vivo analysis of autophagy in response to nutrient starvation using transgenic mice expressing a fluorescent autophagosome marker. *Mol Biol Cell* 2004; **15**: 1101–11
- 42 Zheng Q, Su H, Ranek MJ, Wang X. Autophagy and p62 in cardiac proteinopathy. *Circ Res* 2011; **109**: 296–308
- 43 Weihl CC, Iyadurai S, Baloh RH, Pittman SK, Schmidt RE, Lopate G, Pestronk A, Harms MB. Autophagic vacuolar pathology in desminopathies. *Neuromuscul Disord* 2015; **25**: 199–206
- 44 Clemen CS, Fischer D, Reimann J, Eichinger L, Müller CR, Müller HD, Goebel HH, Schröder R. How much mutant protein is needed to cause a protein aggregate myopathy in vivo? Lessons from an exceptional desminopathy. *Hum Mutat* 2009; **30**: E490–9
- 45 Schröder R, Schoser B. Myofibrillar myopathies: a clinical and myopathological guide. *Brain Pathol* 2009; **19**: 483–92
- 46 Ruparelia AA, Oorschot V, Ramm G, Bryson-Richardson RJ. FLNC myofibrillar myopathy results from impaired autophagy and protein insufficiency. *Hum Mol Genet* 2016; **25**: 2131–42
- 47 Arndt V, Dick N, Tawo R, Dreiseidler M, Wenzel D, Hesse M, Fürst DO, Saftig P, Saint R, Fleischmann BK, Hoch M. Chaperone-assisted selective autophagy is essential for muscle maintenance. *Curr Biol* 2010; **20**: 143–8
- 48 Laskowska E, Matuszewska E, Kuczynska-Wisnik D. Small heat shock proteins and protein-misfolding diseases. *Curr Pharm Biotechnol* 2010; **11**: 146–57
- 49 Bennardini F, Wrzosek A, Chiesi M. Alpha B-crystallin in cardiac tissue. Association with actin and desmin filaments. *Circ Res* 1992; **71**: 288–94
- 50 Kawano F, Fujita R, Nakai N, Terada M, Ohira T, Ohira Y. HSP25 can modulate myofibrillar desmin cytoskeleton following the phosphorylation at Ser15 in rat soleus muscle. *J Appl Physiol* 2012; **112**: 176–86
- 51 Maerkens A, Kley RA, Olive M, Theis V, van der Ven PF, Reimann J, Milting H, Schreiner A, Uszkoreit J, Eisenacher M, Barkovits K. Differential proteomic analysis of abnormal intramyoplasmic aggregates in desminopathy. *J Proteomics* 2013; **90**: 14–27
- 52 Sharma S, Conover GM, Elliott JL, Der Perng M, Herrmann H, Quinlan RA. alphaB-crystallin is a sensor for assembly intermediates and for the subunit topology of desmin intermediate filaments. *Cell Stress Chaperones* 2017; **22**: 613–26
- 53 Tucker NR, Shelden EA. Hsp27 associates with the titin filament system in heat-shocked zebrafish cardiomyocytes. *Exp Cell Res* 2009; **315**: 3176–86
- 54 Nicholls P, Bujalowski PJ, Epstein HF, Boehning DF, Barral JM, Oberhauser AF. Chaperone-mediated reversible inhibition of the sarcomeric myosin power stroke. *FEBS Lett* 2014; **588**: 3977–81
- 55 Codina M, Li J, Gutierrez J, Kao JP, Du SJ. Loss of Smyhc1 or Hsp90alpha1 function results in different effects on myofibril organization in skeletal muscles of zebrafish embryos. *PLoS ONE* 2010; **5**: e8416
- 56 Hawkins TA, Haramis AP, Etard C, Prodromou C, Vaughan CK, Ashworth R, Ray S, Behra M, Holder N, Talbot WS, Pearl LH. The ATPase-dependent chaperoning activity of Hsp90a regulates thick filament formation and integration during skeletal muscle myofibrillogenesis. *Development* 2008; **135**: 1147–56
- 57 Srikakulam R, Winkelmann DA. Chaperone-mediated folding and assembly of myosin in striated muscle. *J Cell Sci* 2004; **117**: 641–52
- 58 Barral JM, Hutagalung AH, Brinker A, Hartl FU, Epstein HF. Role of the myosin assembly protein UNC-45 as a molecular chaperone for myosin. *Science* 2002; **295**: 669–71
- 59 Voelkel T, Andresen C, Unger A, Just S, Rottbauer W, Linke WA. Lysine methyltransferase Smyd2 regulates Hsp90-mediated protection of the sarcomeric titin springs and cardiac function. *Biochim Biophys Acta* 2013; **1833**: 812–22

- 60 Donlin LT, Andresen C, Just S, Rudensky E, Pappas CT, Kruger M, Jacobs EY, Unger A, Zieseniss A, Dobenecker MW, Voelkel T. Smyd2 controls cytoplasmic lysine methylation of Hsp90 and myofilament organization. *Genes Dev* 2012; **26**: 114–19
- 61 Paulsen G, Lauritzen F, Bayer ML, Kallhovde JM, Ugelstad I, Owe SG, Hallen J, Bergersen LH, Raastad T. Subcellular movement and expression of HSP27, alphaB-crystallin, and HSP70 after two bouts of eccentric exercise in humans. *J Appl Physiol* 1985; **2009**: 570–82
- 62 Rivas-Pardo JA, Eckels EC, Popa I, Kosuri P, Linke WA, Fernandez JM. Work done by titin protein folding assists muscle contraction. *Cell Rep* 2016; **14**: 1339–47
- 63 Sanbe A, Daicho T, Mizutani R, Endo T, Miyauchi N, Yamauchi J, Tanonaka K, Glabe C, Tanoue A. Protective effect of geranylgeranylacetone via enhancement of HSPB8 induction in desmin-related cardiomyopathy. *PLoS ONE* 2009; **4**: e5351
- 64 Wang X, Klevitsky R, Huang W, Glasford J, Li F, Robbins J. AlphaB-crystallin modulates protein aggregation of abnormal desmin. *Circ Res* 2003; **93**: 998–1005
- 65 Lomiwes D, Hurst SM, Dobbie P, Frost DA, Hurst RD, Young OA, Farouk MM. The protection of bovine skeletal myofibrils from proteolytic damage post mortem by small heat shock proteins. *Meat Sci* 2014; **97**: 548–57

Received 29 May 2018

Accepted after revision 17 August 2018

Published online Article Accepted on 4 September 2018